Species heterogeneity and synergy to boost photocatalytic hydrogen evolution

Jiankang Zhang,[a,#] Panzhe Qiao,[b,#] Hao Tan,[c] Lin Cui,[a] Zhan Zhou,[d] Dong Lin,[e] Yongxiao Tuo,[f,*] Yong Qin[a,g,*]

[a] Interdisciplinary Research Center of Biology & Catalysis, School of Life Sciences, Northwestern Polytechnical University, Xi'an 710072, P. R. China

[b] Shanghai Synchrotron Radiation Facility, Shanghai Advanced Research Institute, Chinese Academy of Science, Shanghai 201210, P. R. China

[c] School of Materials Science and Engineering, Peking University, Beijing 100871, P. R. China

[d] College of Chemistry and Chemical Engineering, Henan Key Laboratory of Function-Oriented Porous Materials, Luoyang Normal University, Luoyang 471934, P. R. China

[e] Max Planck-Cardiff Centre on the Fundamentals of Heterogeneous Catalysis FUNCAT, Cardiff Catalysis Institute, School of Chemistry, Cardiff University, Cardiff CF103AT, United Kingdom

[f] State Key Laboratory of Heavy Oil Processing, College of New Energy, China University of Petroleum (East China), Qingdao 266580, P. R. China

[g] State Key Laboratory of Coal Conversion, Institute of Coal Chemistry, Chinese Academy of Sciences, Taiyuan 030001, P. R. China

[#] These authors contributed equally to this work.

[*] Corresponding authors. E-mail addresses: yxtuo@upc.edu.cn; qinyong@nwpu.edu.cn

Density Functional Theory calculations

Density Functional Theory (DFT) calculations were performed by the Vienna Ab-initio Simulation Package (VASP) with the projector augmented wave (PAW) method. The model optimization and electron exchange-correlation were processed using the generalized gradient approximation (GGA) of Perdew-Burke Ernzerhof (PBE) functional. Before the calculation, the energy cutoff and Brillouin zone were optimized and set as 400 eV and 3×3×1 k-point mesh, respectively. The convergence energy criterion was 1×10^{-4} eV for the self-consistent calculations. The convergence force criterion was 0.03 eV $Å^{-1}$ for the stress on each atom after the ionic relaxation. All calculations were non-spin polarized.

The stable (101) facet of TiO_2 assembled by a (1×3) unit was chosen to support Pt atoms with a vacuum region of 15 Å. According to the previous study, Pt single atom (Pt_{SA} or Pt_1) prefers to binding on the bridge site between two edge 2-fold-coordinated oxygen atoms (O_{2c}) of TiO_2(101) surface[1,2]. Pt nanocluster (Pt_{NC} or Pt_4) prefers to binding with three O_{2c} sites of TiO_2(101) surface with a tetrahedral form[3]. The optimized configurations of Pt_1/TiO_2(101) and Pt_4/TiO_2(101) in this study are consistent with the previously reported results, which represent Pt_{SA}@TiO_2 and Pt_{SA}@TiO_2 photocatalysts, respectively. Pt_1 and Pt_4 were simultaneously deposited on the TiO_2(101) surface to represent the Pt_{SA+NC}@TiO_2 photocatalyst. Then the formation of oxygen vacancy on the Pt_1-Pt_4/TiO_2(101) were simulated and evaluated, and the O_{2c} oxygen site interacting with Pt_4 prefers to generate the vacancy than the other oxygen sites. This computational result appears to differ from previous research, where subsurface Ov were more stable than surface Ov. This discrepancy may arise from the presence of Pt, which forms bonds with unsaturated Ti atoms at the surface Ov sites, thereby stabilizing surface Ov and rendering them more stable than subsurface Ov. This aligns with previous research that indicates molecular adsorption can reverse the stability of both types of Ov.[4] The obtained photocatalyst model was named as Pt_{SA+NC}@TiO_2-Ov.

For the calculations of alkaline hydrogen evolution process, we considered two key reaction steps based on the previous study and our experimental results[5]:

$$H_2O + e^- + * \rightarrow H^* + OH^- \quad (1)$$

$$2H^* \rightarrow H_2 \uparrow \tag{2}$$

The free energy is defined as:

$$\Delta G = \Delta E_{ads} + \Delta E_{ZPE} - T\Delta S_{ads} \tag{3}$$

where ΔE_{ads} is the adsorption energy, ΔE_{ZPE} is the zero point energy difference between adsorbed and gaseous species, and $T\Delta S_{ads}$ is the corresponding entropy difference between these two states (T is set to be 298 K).

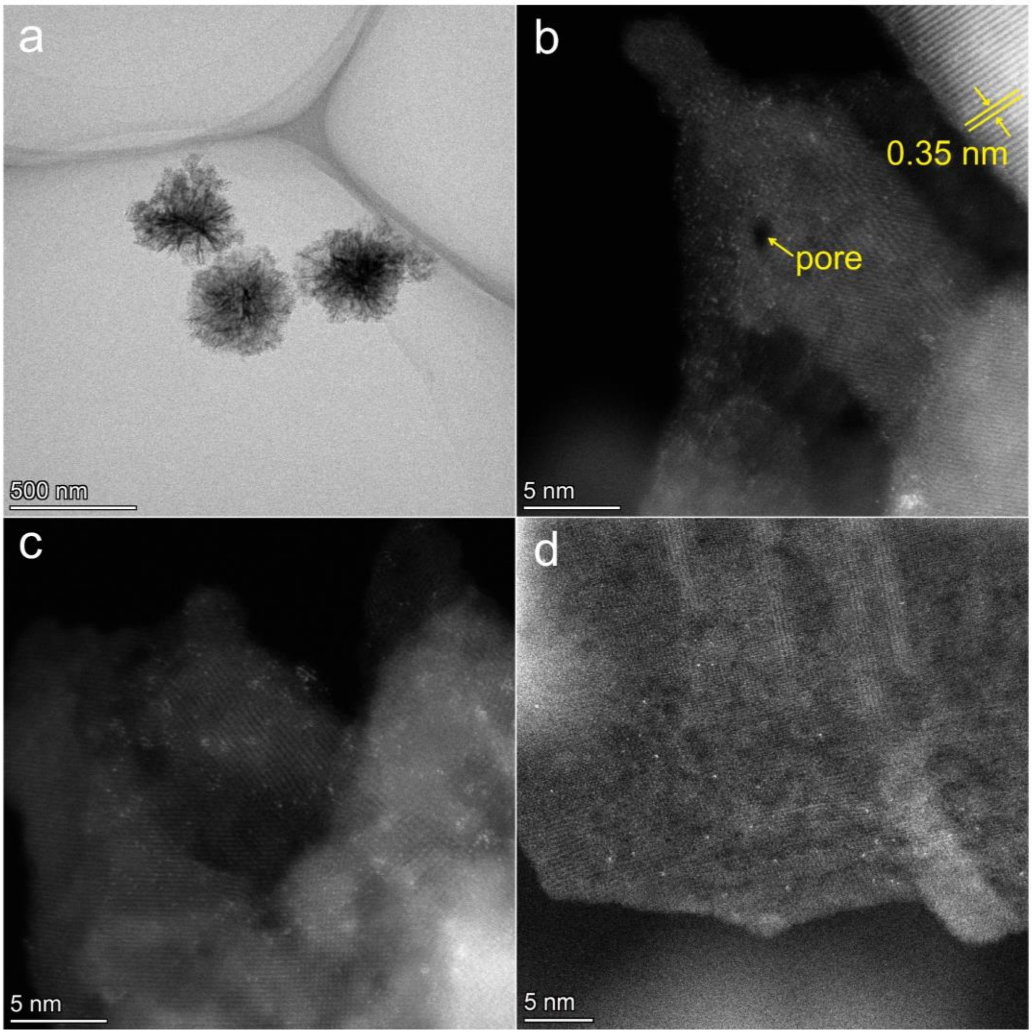

Figure S1. (a) TEM and (b-d) HAADF-STEM images of the Pt_{SA}@TiO_2 photocatalysts. The hierarchical spheres are composed of thin nanosheets (also see Figures S2a and S3a), whose edges are almost transparent.

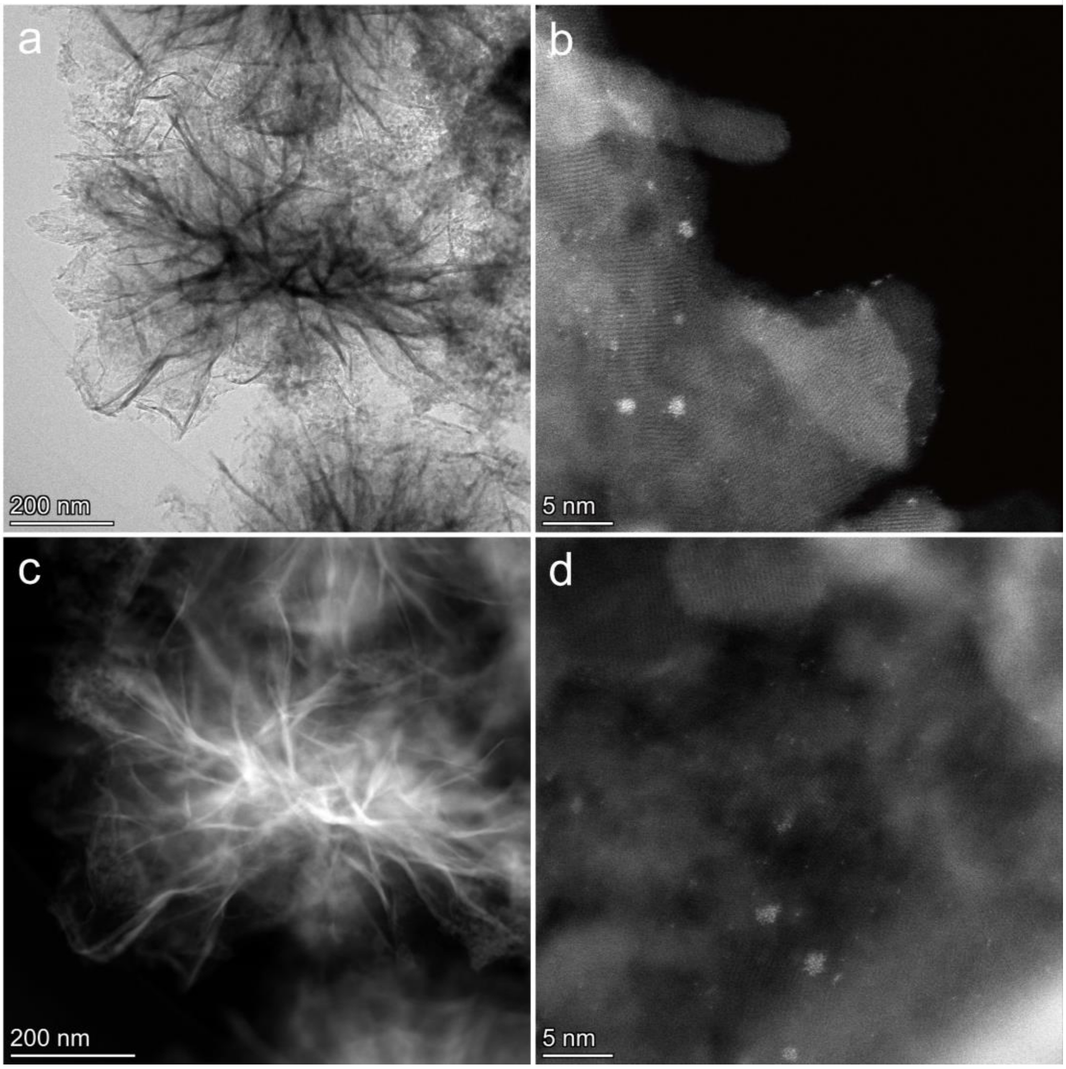

Figure S2. (a) TEM and (b-d) HAADF-STEM images of the Pt_{SA+NC}@TiO_2 photocatalysts.

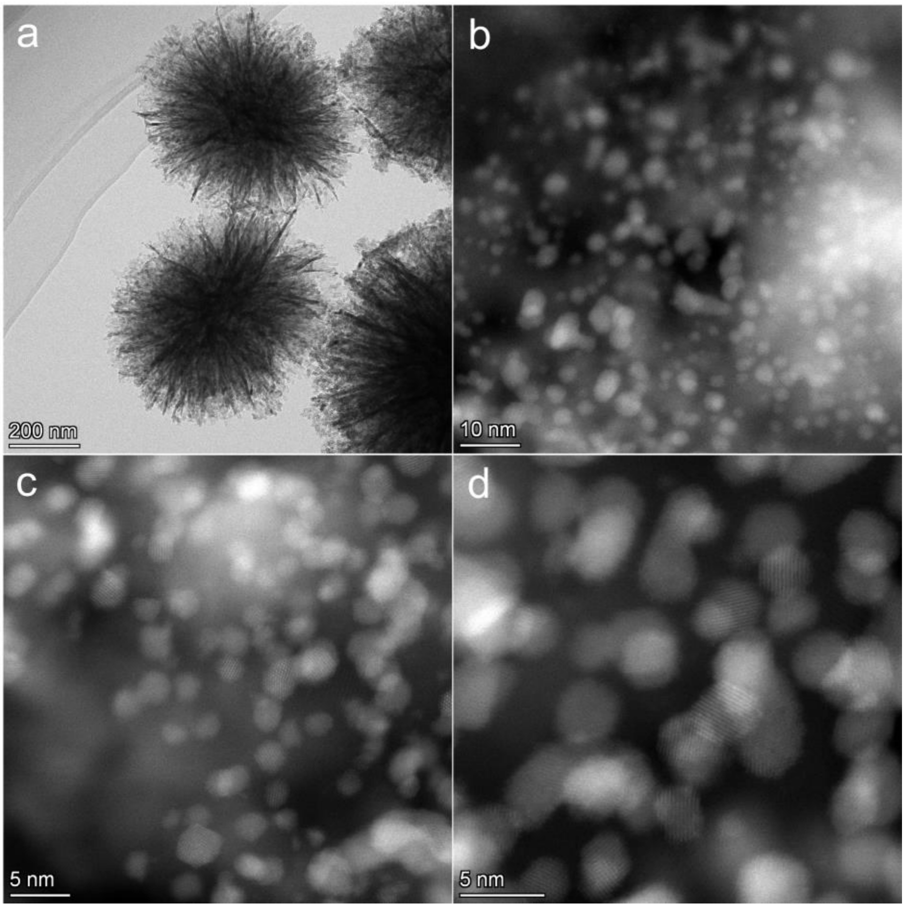

Figure S3. (a) TEM and (b-d) HAADF-STEM images of the Pt_{NP}@TiO_2 photocatalysts.

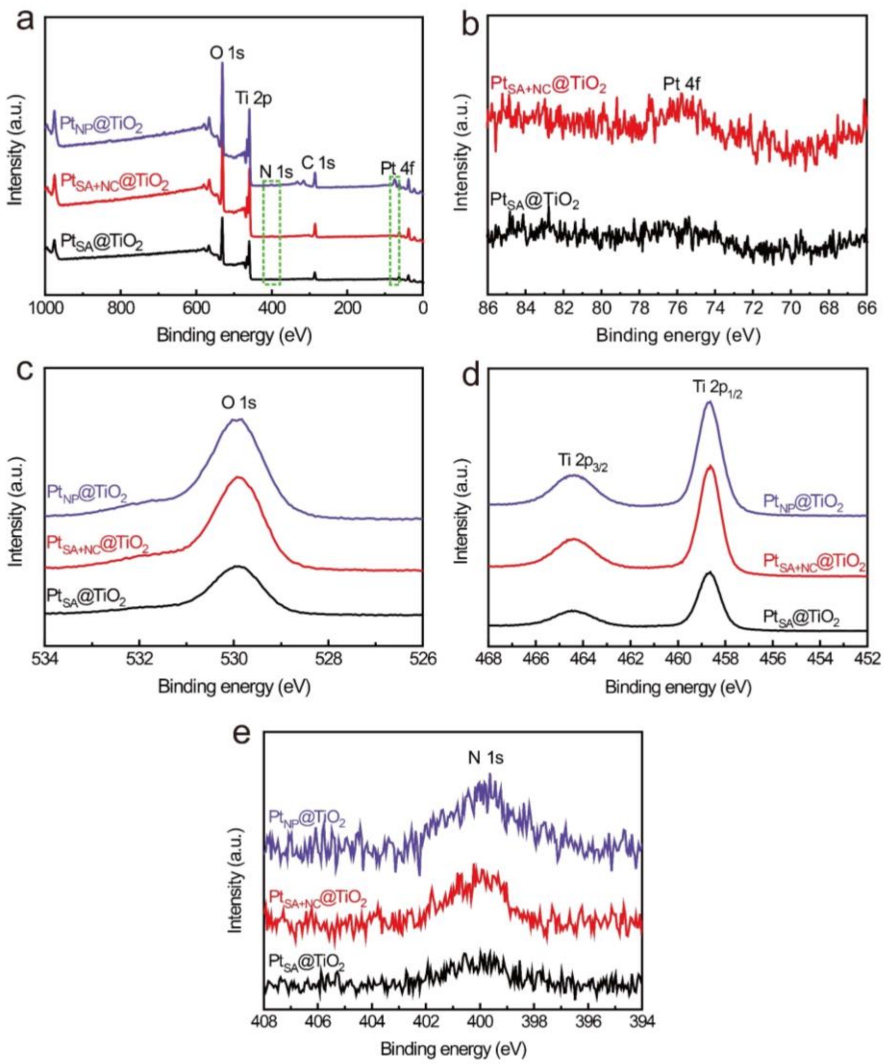

Figure S4. XPS (a) survey, (b) Pt 4f, (c) O 1s, (d) Ti 2p and (e) N 1s spectra of the as-prepared photocatalysts.

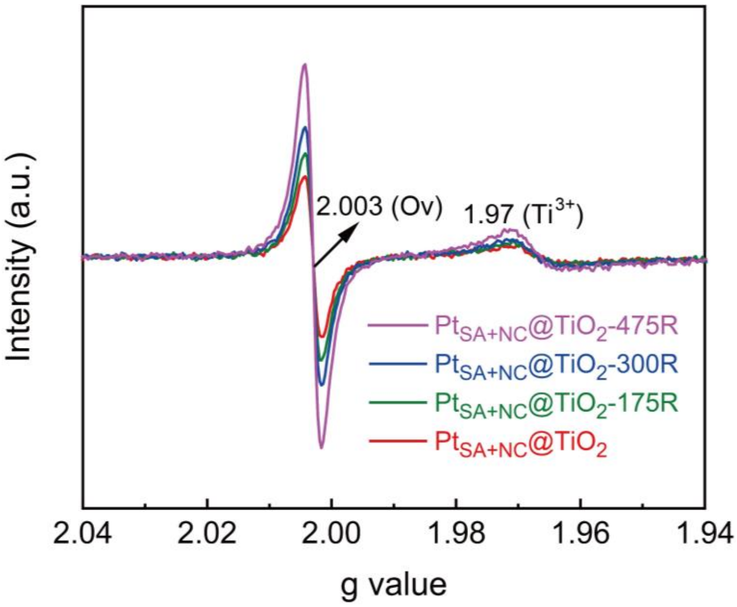

Figure S5. EPR spectra of the photocatalysts obtained at 77 K.

Figure S6. The color comparison of the two photocatalysts under the same reduction conditions.

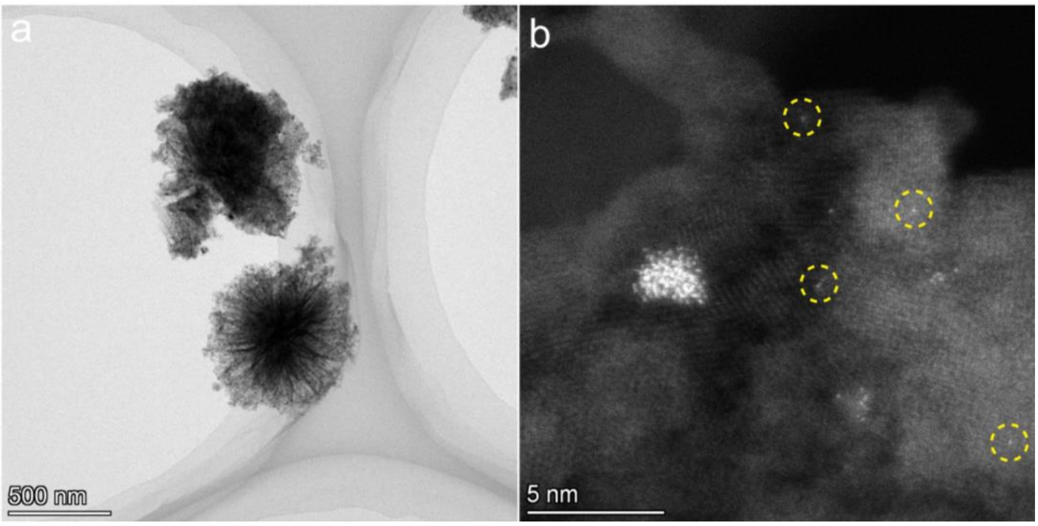

Figure S7. (a) TEM and (b) HAADF-STEM images of the Pt_{SA+NC}@TiO_2-175R photocatalysts.

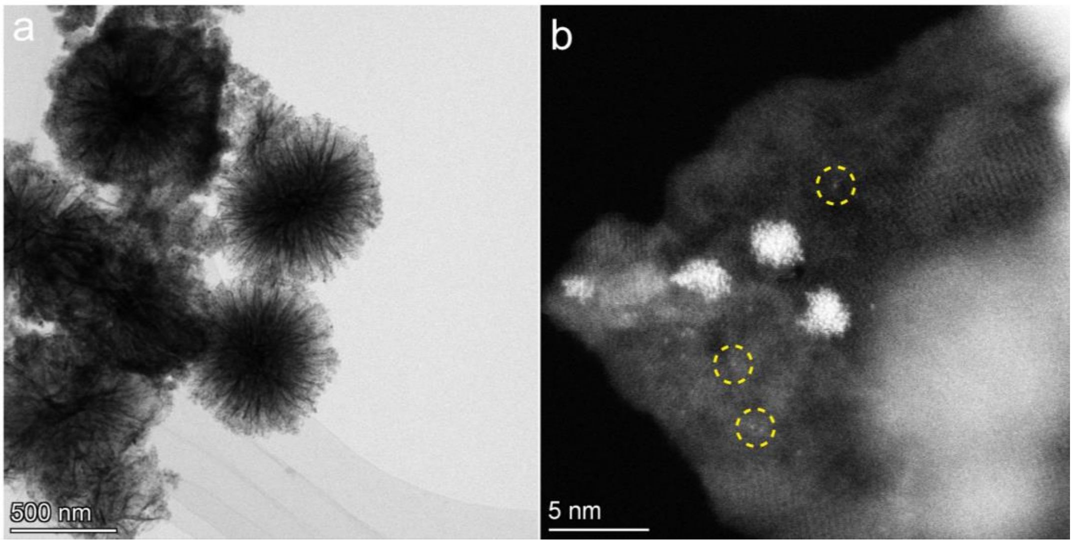

Figure S8. (a) TEM and (b) HAADF-STEM images of the Pt_{SA+NC}@TiO_2-300R photocatalysts.

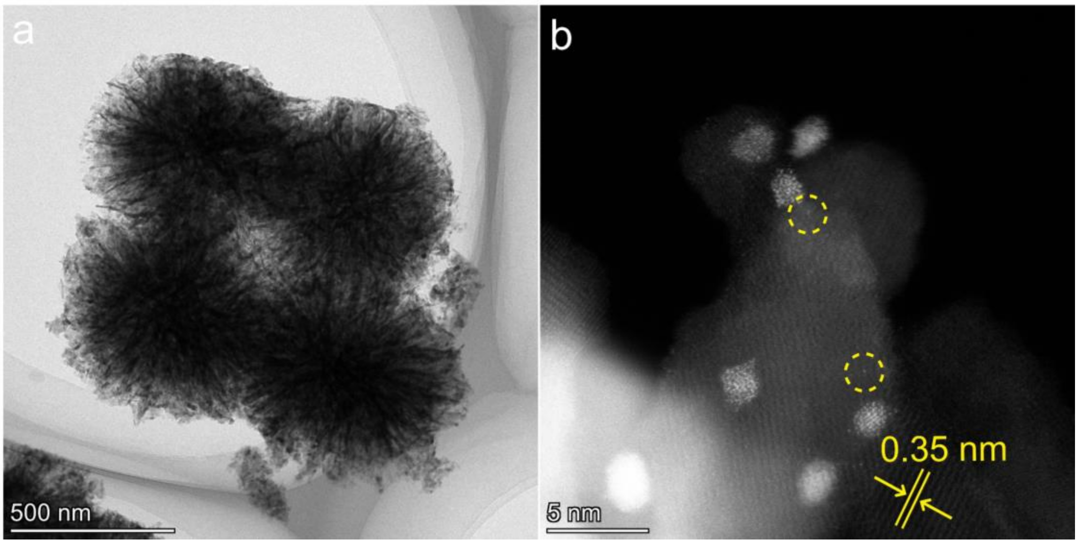

Figure S9. (a) TEM and (b) HAADF-STEM images of the Pt_{SA+NC}@TiO_2-475R photocatalysts.

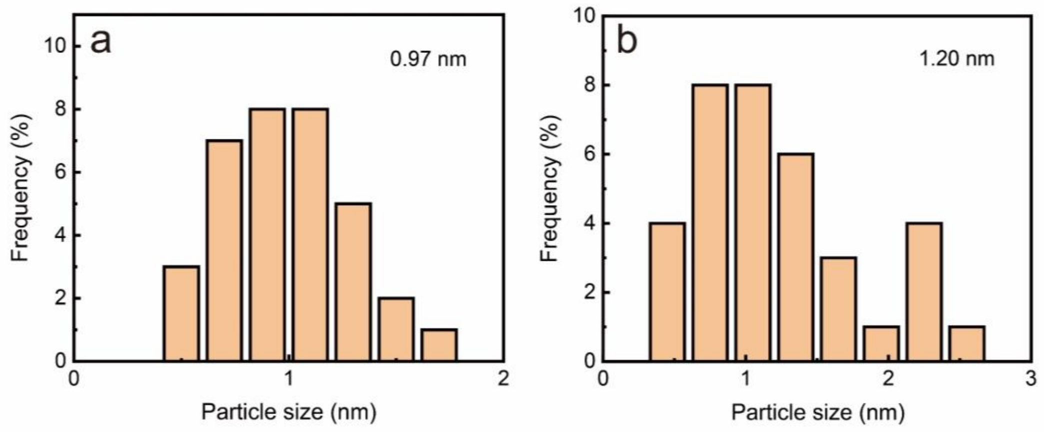

Figure S10. Particle size distribution of the Pt@TiO_2-175R and Pt@TiO_2-475R photocatalysts.

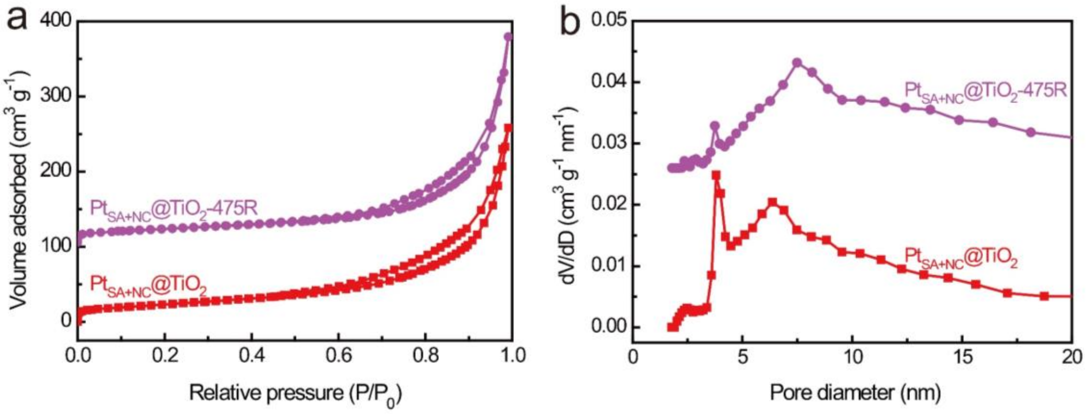

Figure S11. (a) N_2 adsorption–desorption isotherms and (b) the corresponding pore size distribution curves of the two photocatalysts.

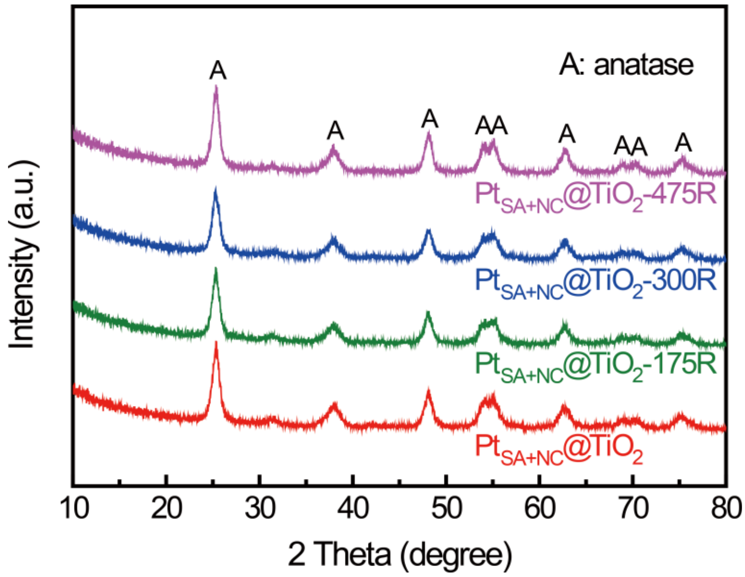

Figure S12. XRD patterns of the photocatalysts. There is no observable change in view of the structures of the photocatalysts.

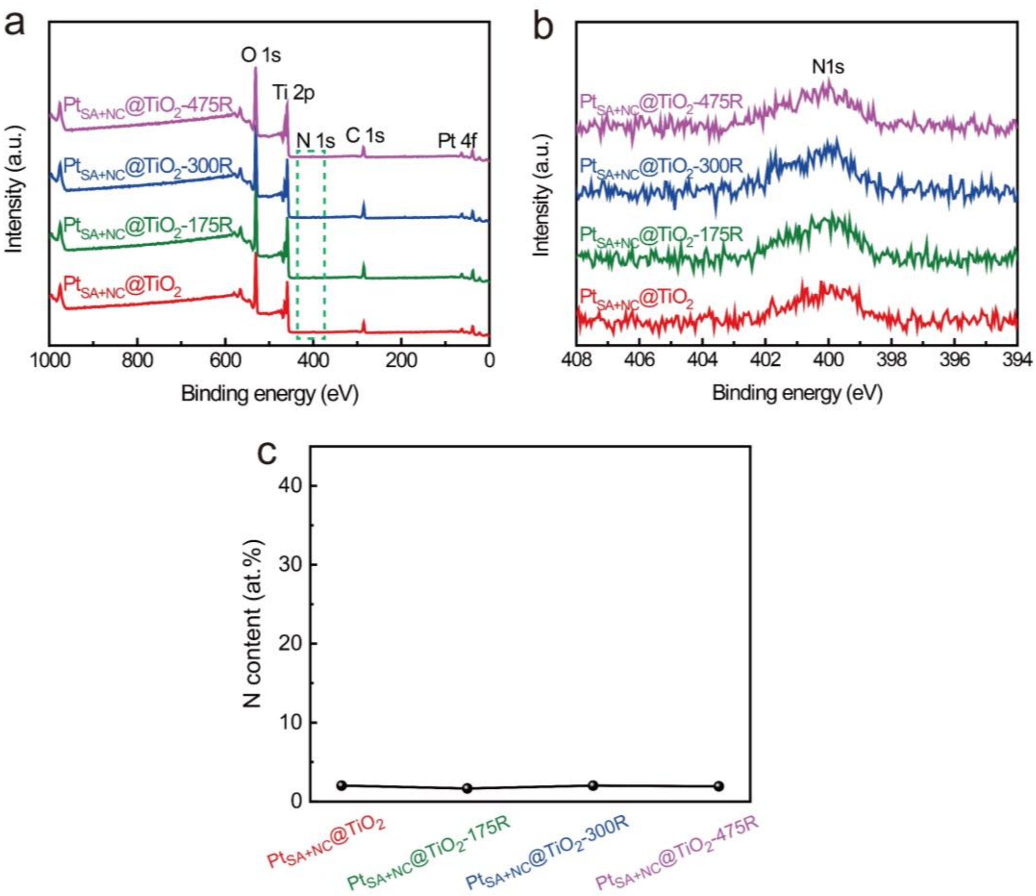

Figure S13. XPS (a) survey and (b) N 1s spectra of the four photocatalysts. (c) The corresponding N content (determined from XPS) over the photocatalysts.

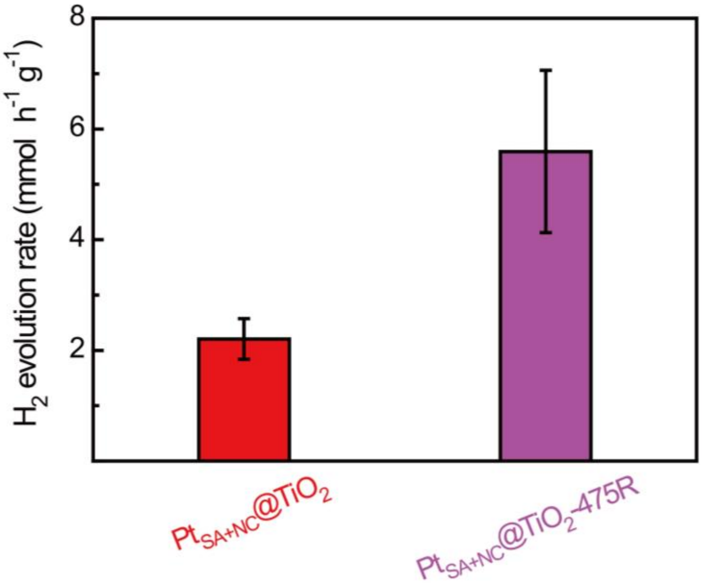

Figure S14. The H_2 evolution rates from pure methanol over the photocatalysts under UV-Vis light irradiation (20 mA).

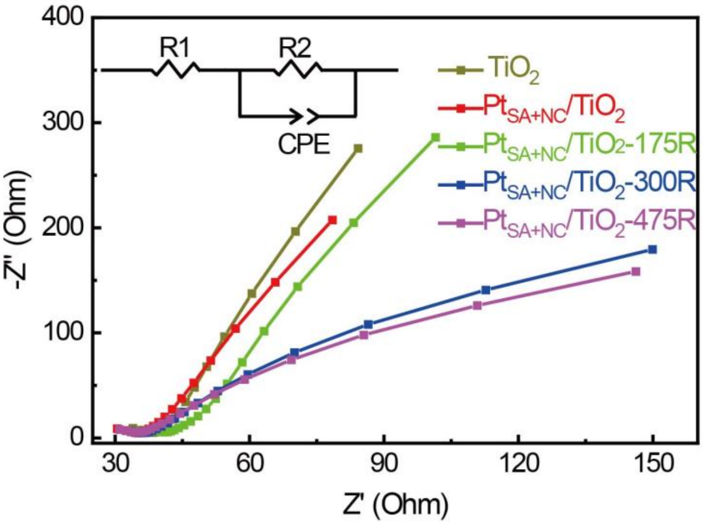

Figure S15. EIS Nyquist plots of the photocatalysts.

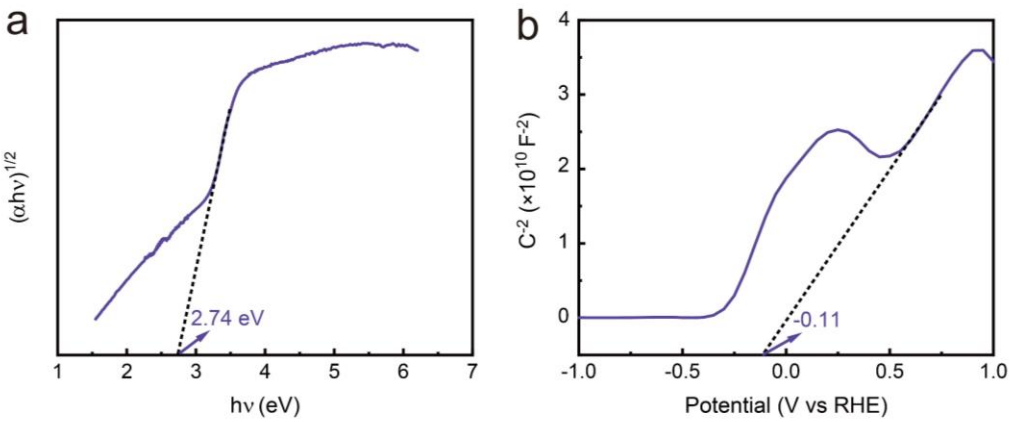

Figure 16. (a) The bandgap energy and (b) Mott-Schottky plot of the Pt_{SA+NC}@TiO_2-475R photocatalyst.

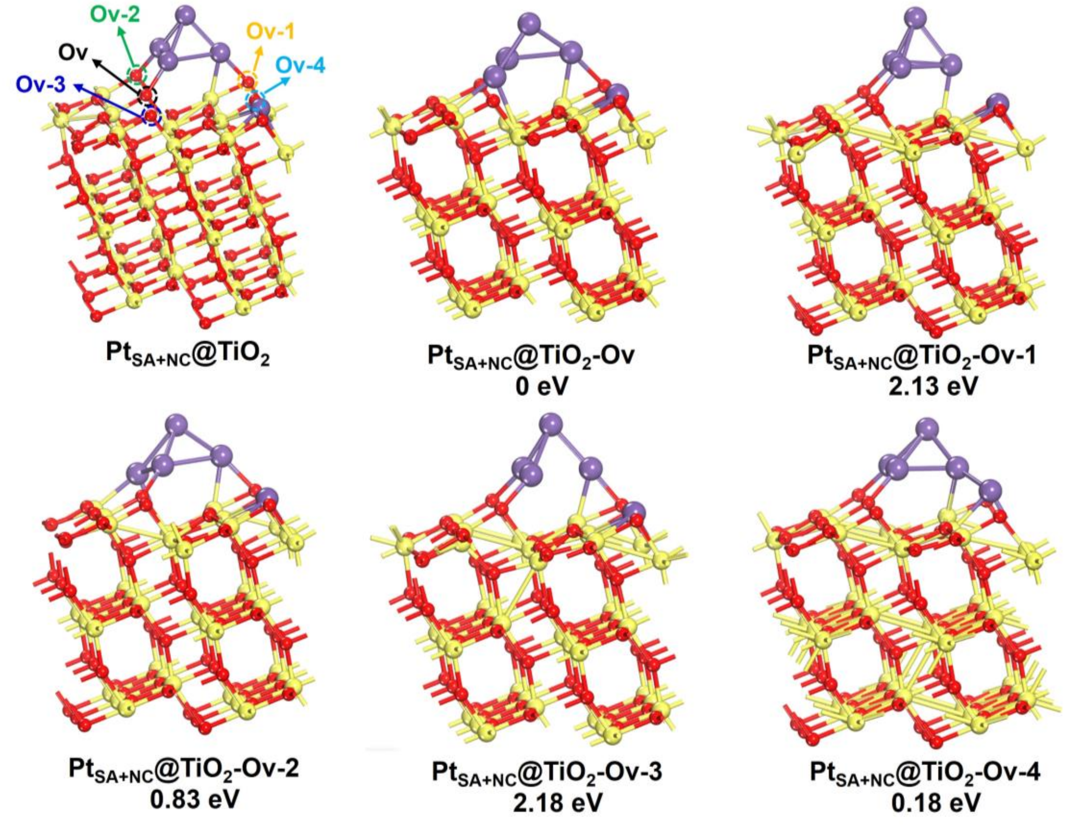

Figure S17. The optimized configurations of Pt$_{SA+NC}$@TiO$_2$-Ov photocatalysts with different Ov on the TiO$_2$ surface and the corresponding relative energy.

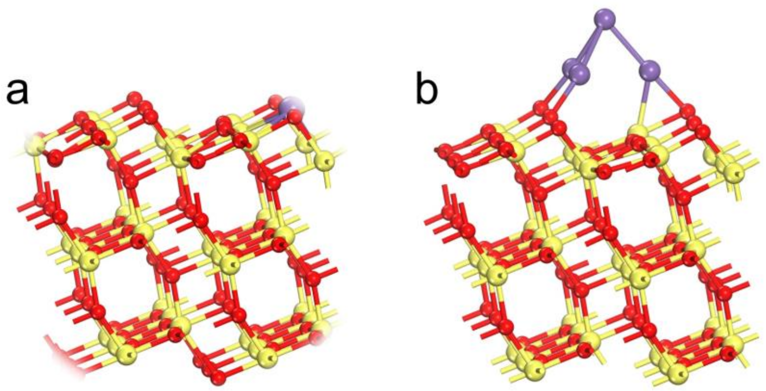

Figure S18. The optimized configurations of (a) Pt_{SA}@TiO_2 and (b) Pt_{NC}@TiO_2 photocatalysts, respectively.

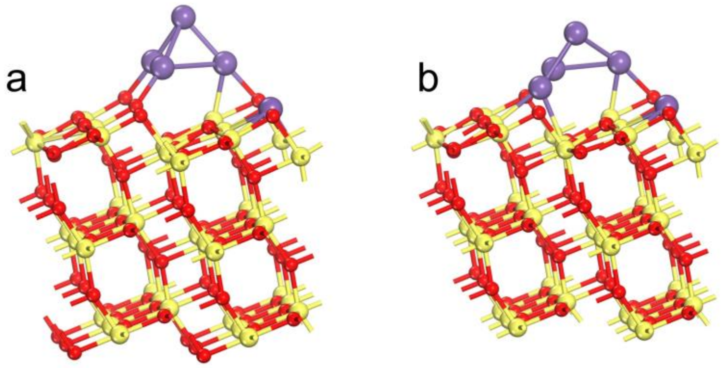

Figure S19. The optimized configurations of (a) Pt_{SA+NC}@TiO_2 and (b) Pt_{SA+NC}@TiO_2-Ov photocatalysts, respectively.

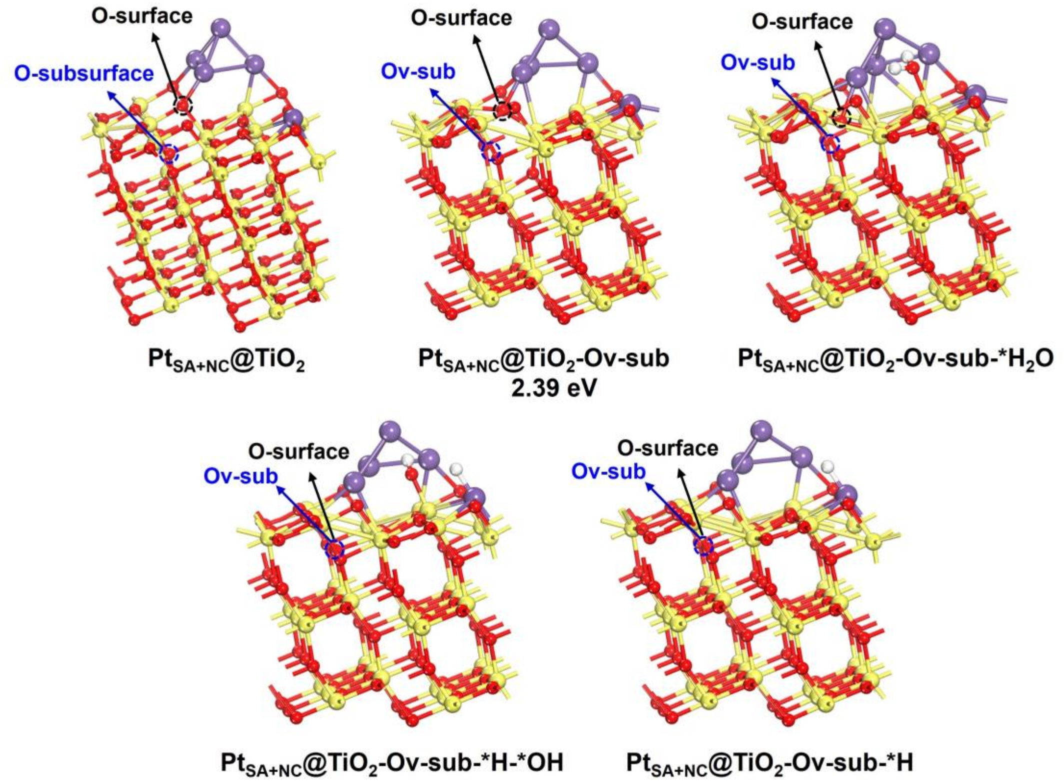

Figure S20. The optimized configurations of $Pt_{SA+NC}@TiO_2$-Ov-sub and *H_2O, *H−*OH and *H adsorbed on the $Pt_{SA+NC}@TiO_2$-Ov-sub.

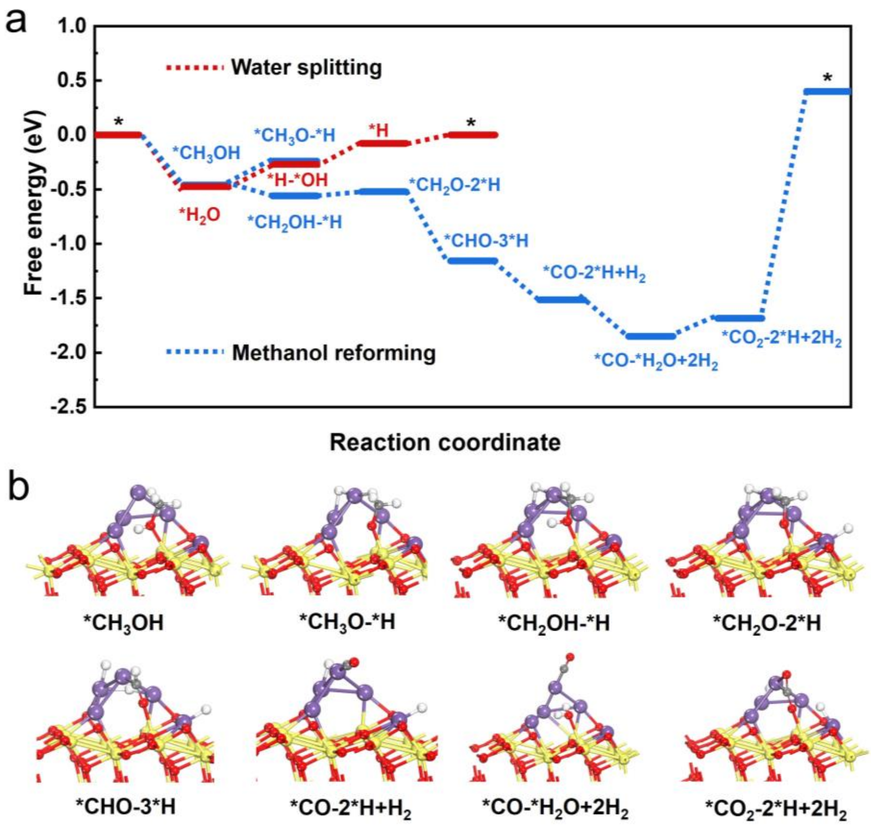

Figure S21. (a) The comparison of reaction energy for water splitting process and methanol photocatalytic reforming process over the Pt_{SA+NC}@TiO_2-Ov photocatalysts. (b) The optimized configurations of the reaction intermediates.

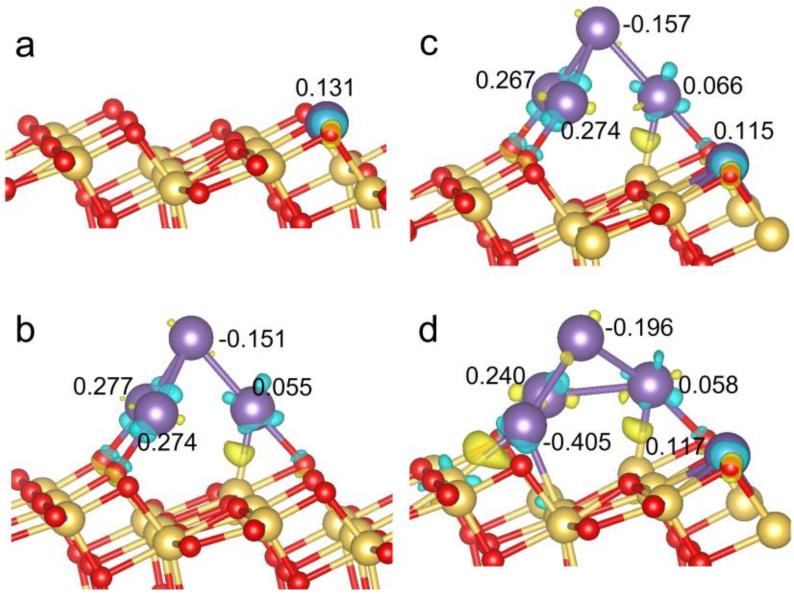

Figure S22. (f) Three-dimensional charge density difference of Pt on the (a) Pt_{SA}@TiO_2, (b) Pt_{NC}@TiO_2, (c) Pt_{SA+NC}@TiO_2 and (d) Pt_{SA+NC}@TiO_2-Ov photocatalysts with isosurface value of 0.03 eV·Å^{-3} (The unit is eV for the digits). The yellow and blue isosurfaces indicate the electron accumulation and depletion, respectively.

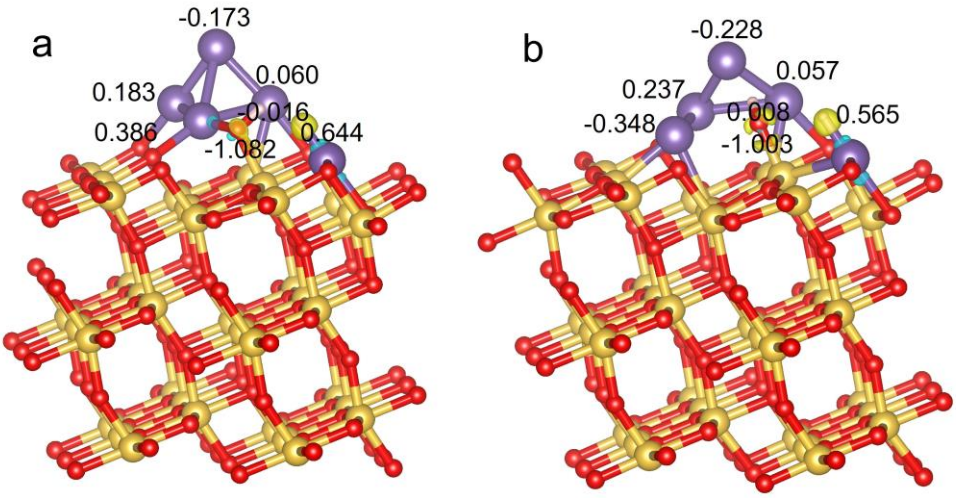

Figure S23. Charge transfer between Pt and *OH/*H species after water splitting on (a) Pt_{SA+NC}@TiO_2 and (b) Pt_{SA+NC}@TiO_2-Ov. The isosurface value is 0.03 eV·Å^{-3}, and the yellow and blue isosurfaces indicate the electron accumulation and depletion, respectively.

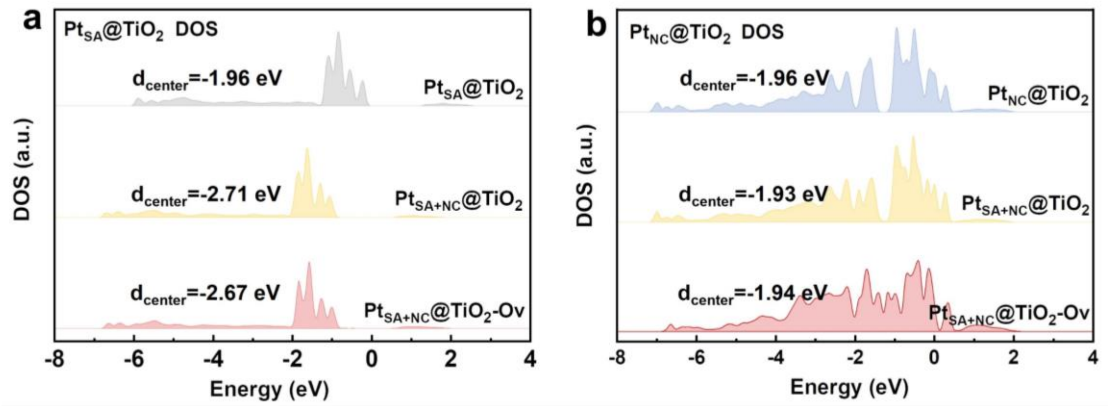

Figure S24. DOS of (a) Pt SA and (b) Pt NC in Pt$_{SA}$@TiO$_2$, Pt$_{SA+NC}$@TiO$_2$ and Pt$_{SA+NC}$@TiO$_2$-Ov photocatalysts.

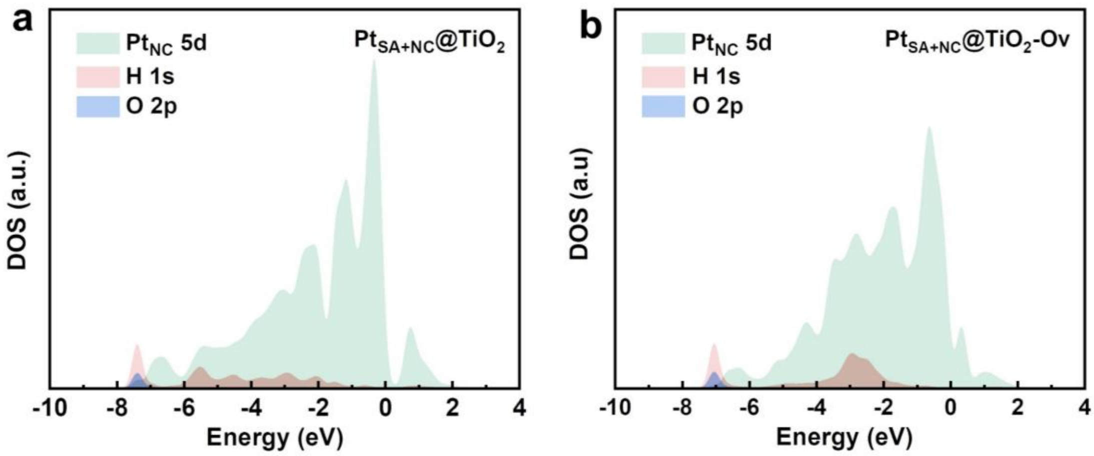

Figure S25. DOS of Pt_{NC} 5d, H 1s and O 2p atom of *OH in *H–*OH adsorbed on (a) Pt_{SA+NC}@TiO_2 and (b) Pt_{SA+NC}@TiO_2-Ov photocatalysts.

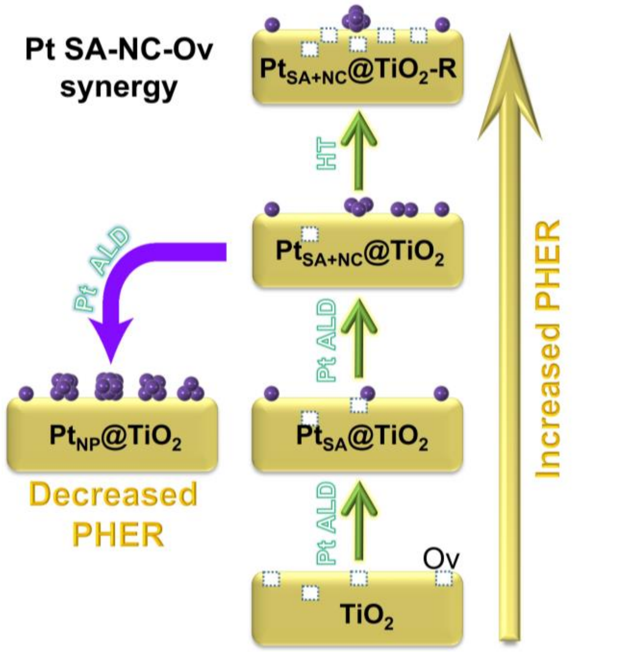

Figure 26. Schematic of the structure–activity relationship of the photocatalysts synthesized by ALD (HT represents high-temperature treatment).

Table S1. Summary of the structure parameters, Pt content, PHE rates and TOF values of the photocatalysts.

Photocatalysts	S_{BET} ($m^2\ g^{-1}$)	Pore volume ($m^3\ g^{-1}$)	Mean size (nm)[a]	Pt content (wt.%)[b]	PHE rate (mmol $h^{-1}\ g^{-1}$)[c]	TOF (h^{-1})
TiO_2	76	0.44	--	--	0.08	--
$Pt_{SA}@TiO_2$	83	0.37	--	0.012	0.39	632
$Pt_{SA+NC}@TiO_2$	85	0.39	0.95	0.034	3.94	2260
$Pt_{NP}@TiO_2$	80	0.40	1.61	1.78	3.36	37
$Pt_{SA+NC}@TiO_2$-175R	--	--	0.97	0.034	4.82	2768
$Pt_{SA+NC}@TiO_2$-300R	--	--	1.15	0.034	5.97	3428
$Pt_{SA+NC}@TiO_2$-475R	67	0.42	1.20	0.034	6.35	3645

[a] The mean particle size values were calculated by the NCs/NPs, i.e., SAs are not included.

[b] The Pt content was obtained from ICP-OES.

[c] The H_2 evolution rates were determined based on the overall amount of the photocatalysts.

Table S2. EXAFS fitting parameters at the Pt L_3-edge for various samples.

Samples	shell	CN[a]	R(Å)[b]	σ^2(Å^2)[c]	ΔE_0 (eV)[d]	R factor
Pt foil	Pt-Pt	12	2.76	--	--	0.003
PtO_2	Pt-O	6	2.01	--	--	0.016
Pt_{SA+NC}@TiO_2	Pt-O	2.8	1.95	8.4±9.1	7.2	0.017
	Pt-Pt	1.9	2.71	7.0±6.4	-5.2	
Pt_{SA+NC}@TiO_2-300R	Pt-O	2.6	1.92	5.8±8.1	5.8	0.018
	Pt-Pt	2.4	2.73	5.0±6.3	2.5	
Pt_{SA+NC}@TiO_2-475R	Pt-O	1.4	1.96	5.6±6.5	6.9	0.010
	Pt-Pt	4.5	2.75	6.8±4.2	3.5	

[a]*N*: coordination numbers; [b]*R*: bond distance; [c]σ^2: Debye-Waller factors; [d] ΔE_0: the inner potential correction. *R* factor: goodness of fit. S_0^2 was set to 0.820, according to the experimental EXAFS fit of Pt foil reference by fixing CN as the known crystallographic value.

Table S3. Comparison of the photocatalytic H_2 evolution activity over the relevant Pt-based photocatalysts.

Photocatalysts	Light source	Sacrificial agents	Pt loadings (wt%)	TOF (h^{-1})	PHE rates [a] (mmol h^{-1} g^{-1})	Ref.
Pt-SA/C_3N_4	300 W Xe lamp	10% CH_3OH	0.11	250	1.4	[6]
Pt-SA/C_3N_4 Pt-NP/C_3N_4	300 W Xe lamp	10% TEOA	0.16 3.2	775 83	6.36 13.62	[7]
SA-Pt/g-C_3N_4-8.7	300 W Xe lamp	10% TEOA	8.7	50.1 [b]	22.65	[8]
Pt_5/CdS	300 W Xe lamp	20% TEOA	0.75	--	13	[9]
Pt_{SA+NC}/TiO_2-475R	300 W Xe lamp	20% CH_3OH	0.034	3645 8871	3.94 (5 °C) 15.46 (25 °C)	This work
TiO_2-BNS-$Pt_{0.05}$	150 W Xe lamp	50% CH_3OH	0.05	--	0.6887	[10]
0.2Pt/TiO_2	UV/Vis light	30% CH_3OH	0.2	--	8.48	[11]
NYTiO_2-Pt-0.5	300 W Xe lamp	37.5% CH_3OH	0.188	--	20.88	[12]
Pt/TiO_2 Co-O-Pt/TiO_2	300 W Xe lamp	10% CH_3OH 10% CH_3OH	0.1 0.16 Pt+0.18 Co	-- --	22.678 (35 °C) 43.467 (35 °C)	[13]
Pt_1/def-TiO_2	300 W Xe lamp	20% CH_3OH	0.02	51423	52.72	[14]
PtSA-MNSs	300 W Xe lamp	0.1 M AA	12.0	--	11.32	[15]
Pt_1/TiO_2-A	300 W Xe lamp	20% CH_3OH	0.6	--	8.45	[16]
Pt SA/Def-s-TiO_2	300 W Xe lamp	20% CH_3OH	0.57	--	13.46	[17]
Pt1-CN@CuS	150 W Xe lamp	10% CH_3OH	1	--	10.176 (8 °C)	[18]
$Pt_{0.3}$-$ZnIn_2S_4$	300 W Xe lamp	10% TEOA	0.26	--	17.5	[19]
Pt_1@TpPa-1	300 W Xe lamp	4 g L^{-1} SA	0.72	19.5	0.936 (15 °C)	[20]
PtSA-TiO_2 CuSA-TiO_2	500 W/m^2 Xe lamp	CH_3OH	0.64 1.5	-- --	95.3 (40 °C) 101.7 (40 °C)	[21] [c]
Pt-decorated TiO_2 layers	365 nm LED	50% CH_3OH	0.05 mM H_2PtCl_6	357 199 148	-- -- --	[22] [d]
Pt-RC-COF-1	300 W Xe lamp	0.1 M AA	3	--	27.98	[23]

Notes: TEOA, SA and AA represent triethanolamine, sodium ascorbate and ascorbic acid, respectively. The content of sacrificial agents is referred to vol% unless otherwise denoted. The given AQY values in references 9, 10, 11, 13, 19, 20, 21 are 22.5% (420 nm), 25.08% (420 nm), 85.6% (365 nm), 50.3% (LED-530), 50.4% (420 nm), 0.38% (420 nm), respectively.

[a] The reaction temperature is 25 °C unless otherwise denoted.

[b] The value is calculated based on the interlayer confined Pt atom.

[c] The H_2O/methanol ratio is 1:2, and the AQY is 56% for CuSA-TiO_2.

[d] The TOF values of 357, 199 and 148 H_2 $site^{-1}$ s^{-1} is calculated based on Pt SA, Pt atoms (SA + rafts) and all Pt atoms, respectively.

References

(1) Gong, X.-Q.; Selloni, A.; Dulub, O.; Jacobson, P.; Diebold, U. Small Au and Pt clusters at the anatase TiO_2(101) surface: Behavior at terraces, steps, and surface oxygen vacancies. *J. Am. Chem. Soc.* **2008**, *130*, 370−381.
(2) Han, Y.; Liu, C. J.; Ge, Q. Interaction of Pt clusters with the anatase TiO_2 (101) surface: A first principles study. *J. Phys. Chem. B* **2006**, *110*, 7463−7472.
(3) Thang, H. V.; Pacchioni, G.; DeRita, L.; Christopher, P. Nature of stable single atom Pt catalysts dispersed on anatase TiO_2. *J. Catal.* **2018**, *367*, 104−114.
(4) Setvín, M.; Aschauer, U.; Scheiber, P.; Li, Y.-F.; Hou, W.; Schmid, M.; Selloni, A.; Diebold, U. Reaction of O_2 with subsurface oxygen vacancies on TiO_2 anatase (101). *Science*, **2013**, *34*, 988−991.
(5) Zang, Y.; Niu, S.; Wu, Y.; Zheng, X.; Cai, J.; Ye, J.; Xie, Y.; Liu, Y.; Zhou, J.; Zhu, J.; Liu, X.; Wang, G.; Qian, Y. Tuning orbital orientation endows molybdenum disulfide with exceptional alkaline hydrogen evolution capability. *Nat. Commun.* **2019**, *10*, 1217.
(6) Cao, Y.; Wang, D.; Lin, Y.; Liu, W.; Cao, L.; Liu, X.; Zhang, W.; Mou, X.; Fang, S.; Shen, X.; Yao, T. Single Pt atom with highly vacant d-orbital for accelerating photocatalytic H_2 evolution. *ACS Appl. Energy Mater.* **2018**, *1*, 6082−6088.
(7) Li, X.; Bi, W.; Zhang, L.; Tao, S.; Chu, W.; Zhang, Q.; Luo, Y.; Wu, C.; Xie, Y. Single-atom Pt as co-catalyst for enhanced photocatalytic H_2 evolution. *Adv. Mater.* **2016**, *28*, 2427−2431.
(8) Zeng, Z.; Su, Y.; Quan, X.; Choi, W.; Zhang, G.; Liu, N.; Kim, B.; Chen, S.; Yu, H.; Zhang, S. Single-atom platinum confined by the interlayer nanospace of carbon nitride for efficient photocatalytic hydrogen evolution. *Nano Energy* **2020**, *69*, 104409.
(9) Lu, X.; Tong, A.; Luo, D.; Jiang, F.; Wei, J.; Huang, Y.; Jiang, Z.; Lu, Z.; Ni, Y. Confining single Pt atoms from Pt clusters on multi-armed CdS for enhanced photocatalytic hydrogen evolution. *J. Mater. Chem. A* **2022**, *10*, 4594−4600.
(10) Rej, S.; Hejazi, S. M. H.; Badura, Z.; Zoppellaro, G.; Kalytchuk, S.; Kment, Š.; Fornasiero, P.; Naldoni, A. Light-induced defect formation and Pt single atoms synergistically boost photocatalytic H_2 production in 2D TiO_2-bronze nanosheets. *ACS Sustainable Chem. Eng.* **2022**, *10*, 17286−17296.
(11) Xing, J.; Chen, J.; Li, Y.; Yuan, W. T.; Zhou, Y.; Zheng, L.; Wang, H.; Hu, P.; Wang, Y.; Zhao, H.; Wang, Y.; Yang, H. Stable isolated metal atoms as active sites for photocatalytic hydrogen evolution. *Chem. A Eur. J.* **2014**, *20*, 2138−2144.
(12) Jin, J.; Wang, C.; Ren, X.-N.; Huang, S.-Z.; Wu, M.; Chen, L.-H.; Hasan, T.; Wang, B.-J.; Li, Y.; Su, B.-L. Anchoring ultrafine metallic and oxidized Pt nanoclusters on yolk-shell TiO_2 for unprecedentedly high photocatalytic hydrogen production. *Nano Energy* **2017**, *38*, 118−126.
(13) Wang, C.; Wang, K.; Feng, Y.; Li, C.; Zhou, X.; Gan, L.; Feng, Y.; Zhou, H.; Zhang, B.; Qu, X.; Li, H.; Li, J.; Li, A.; Sun, Y.; Zhang, S.; Yang, G.; Guo, Y.; Yang, S.; Zhou, T.; Dong, F.; Zheng, K.; Wang, L.; Huang, J.; Zhang, Z.; Han, X. Co and Pt Dual-single-atoms with oxygen-coordinated Co−O−Pt dimer sites for ultrahigh photocatalytic hydrogen evolution efficiency. *Adv. Mater.* **2021**, *33*, 2003327.
(14) Chen, Y.; Ji, S.; Sun, W.; Lei, Y.; Wang, Q.; Li, A.; Chen, W.; Zhou, G.; Zhang, Z.; Wang, Y.; Zheng, L.; Zhang, Q.; Gu, L.; Han, X.; Wang, D.; Li, Y. Engineering atomic interface by single Pt atoms for enhanced photocatalytic hydrogen production. *Angew. Chem. Int. Ed.* **2020**, *132*, 1311−1317.
(15) Zuo, Q.; Liu, T.; Chen, C.; Ji, Y.; Gong, X.; Mai, Y.; Zhou, Y. Ultrathin metal−organic

framework nanosheets with ultrahigh loading of single Pt atoms for efficient visible-light-driven photocatalytic H_2 evolution. *Angew. Chem. Int. Ed.* **2019**, *58*, 10198−10203.
(16) Sui, Y.; Liu, S.; Li, T.; Liu, Q.; Jiang, T.; Guo, Y.; Luo, J.-L. Atomically dispersed Pt on specific TiO_2 facets for photocatalytic H_2 evolution. *J. Catal.* **2017**, *353*, 250−255.
(17) Hu, X.; Song, J.; Luo, J.; Zhang, H.; Sun, Z.; Li, C.; Zheng, S.; Liu, Q. Single-atomic Pt sites anchored on defective TiO_2 nanosheets as a superior photocatalyst for hydrogen evolution. *J. Energy Chem.* **2021**, *62*, 1−10.
(18) Yan, J.; Ji, Y.; Batmunkh, M.; An, P.; Zhang, J.; Fu, Y.; Jia, B.; Li, Y.; Liu, S.; Ye, J. Breaking platinum nanoparticles to single-atomic Pt-C_4 co-catalysts for enhanced solar-to-hydrogen conversion. *Angew. Chem. Int. Ed.* **2021**, *60*, 2541−2547.
(19) X. Shi, C. Dai, X. Wang, J. Hu, J. Zhang, L. Zheng, L. Mao, H. Zheng, M. Zhu, Protruding Pt single-sites on hexagonal $ZnIn_2S_4$ to accelerate photocatalytic hydrogen evolution, *Nat. Commun.* **2022**, *13*, 1287.
(20) Dong, P.; Wang, Y.; Zhang, A.; Cheng, T.; Xi, X.; Zhang J. Platinum single atoms anchored on a covalent organic framework: Boosting active sites for photocatalytic hydrogen evolution. *ACS Catal.* **2021**, *11*, 13266−13279.
(21) Zhang, Y.; Zhao, J.; Wang, H.; Xiao, B.; Zhang, W.; Zhao, X.; Lv, T.; Thangamuthu, M.; Zhang, J.; Guo, Y.; Ma, J.; Lin, L.; Tang, J.; Huang, R.; Liu, Q. Single-atom Cu anchored catalysts for photocatalytic renewable H_2 production with a quantum efficiency of 56%. *Nat. Commun.* **2022**, *13*, 58.
(22) Qin, S.; Will, J.; Kim, H.; Denisov, N.; Carl, S.; Spiecker, E.; Schmuki, P. Single atoms in photocatalysis: low loading is good enough! *ACS Energy Lett.* **2023**, *8*, 1209−1214.
(23) Zhang, W.; Chen, L.; Dai, S.; Zhao, C.; Ma, C.; Wei, L.; Zhu, M.; Chong, S. Y.; Yang, H.; Liu, L.; Bai, Y.; Yu, M.; Xu, Y.; Zhou, X.; Zhang, Q.; An, S.; Sprick, R. S.; Little, M. C.; Wu, X.; Jiang, S.; Wu, Y.; Zhang, Y.; Tian, H.; Zhu, W.-H.; Cooper, A. I. Reconstructed covalent organic frameworks. *Nature* **2022**, *604*, 72−79.